

# Constant-roll inflation and primordial black holes with Barrow holographic dark energy

Qihong Huang<sup>1a</sup>, Li-Yang Chen<sup>2</sup>, He Huang<sup>3</sup>, Bing Xu<sup>4</sup> and Kaituo Zhang<sup>5</sup>

<sup>1</sup> *School of Physics and Electronic Science,*

*Zunyi Normal University, Zunyi, Guizhou 563006, China*

<sup>2</sup> *College of Physics and Electronic Engineering,*

*Chengdu Normal University, Chengdu, Sichuan 611130, China*

<sup>3</sup> *Institute of Applied Mechanics, Zhejiang University, Hangzhou, Zhejiang 310058, China*

<sup>4</sup> *School of Electrical and Electronic Engineering,*

*Anhui Science and Technology University, Bengbu, Anhui 233030, China*

<sup>5</sup> *Department of Physics, Anhui Normal University, Wuhu, Anhui 241000, China*

## Abstract

We investigate the constant-roll inflation and the evolution of primordial black holes (PBHs) with Barrow holographic dark energy (BHDE). Using the modified Friedmann equation and the constant-roll condition in BHDE model, we calculate the constant-roll parameters, the scalar spectral index and the tensor-to-scalar ratio for the power-law, periodic, and hilltop potential models. By applying Planck 2018 data, the  $r_{0.002} - n_s$  plane analysis under  $\delta = 10^{-4}$  delivers constrained parameter ranges for three inflationary potential models, where the power-law potential imposes  $n \leq 1.1$ , the periodic potential bounds  $f \leq 7$ , and the hilltop potential restricts  $p \leq 4$ . Then, we calculate the primordial curvature perturbation power spectra and PBHs abundance for these models, finding a PBH mass of approximately  $10^{-12}M_{\odot}$  and revealing that these models not only generate sufficient PBHs but also contribute one-third of the dark matter content. Subsequently, we analyze the evolution of PBHs and find that when the effective equation of state parameter evolves from  $1/3$  to  $-1/3$ , the accretion mass increases to approximately  $10^2 M_i$ , while the temperature of the PBHs decreases from  $10^4 K$  to  $10^2 K$ , which indicate that PBHs still exist and can be detected today.

---

<sup>a</sup> Corresponding author: huangqihongzynu@163.com

## I. INTRODUCTION

Inflation, a short period of an exponential accelerating expansion before the radiation dominated era, is the currently widely accepted paradigm of modern cosmology [1, 2]. Inflation not only addresses the puzzles of the standard hot Big Bang cosmology but also provides an explanation for the quantum origin of the Cosmic Microwave Background temperature anisotropies and the Large-Scale Structure [3–5]. In general, a scalar field named as the inflaton field drives the exponential accelerating expansion of the universe during the inflationary epoch. The mechanism of inflation is based on the generation of small quantum fluctuations in the inflaton field. The small quantum fluctuations are amplified in physical scale during the inflationary epoch and lead to a Gaussian, scale-invariant and adiabatic primordial density perturbations [6]. This information is encoded into the primordial scalar power spectrum described by the scalar spectral index  $n_s$ , which is constrained by the Planck 2018 results [7]. In addition, inflation also predicts the generation of tensor perturbations as primordial gravitational waves described by the tensor-to-scalar ratio  $r$  [8]. Usually, the dynamics of inflation is based on the slow-roll approximation, in which the scalar potential is chosen to be nearly flat so that the scalar field can slowly roll down this potential. Once the minimum value of this potential is reached, inflation ends. This scenario is called slow-roll inflation [2, 6, 9], which can be measured by the parameters  $\epsilon_1 = -\dot{H}/H^2$  and  $\epsilon_2 = \ddot{\phi}/H\dot{\phi}$ . For the slow-roll inflation, the small values of the parameters  $\epsilon_1 \ll 1$  and  $\epsilon_2 \ll 1$  are required. If the scalar potential is assumed to be extremely flat, the second condition becomes  $\epsilon_2 = -3$  which corresponds to the ultra slow-roll condition [10–12]. In the ultra slow-roll inflation, the curvature perturbations are not frozen at the super Hubble scales thus leading to non-Gaussianities. Furthermore, when the second condition  $\epsilon_2$  is generalized to be constant, a more generalized scenario named as constant-roll inflation was proposed [13–19], in which the rate of acceleration and velocity of the inflaton field are constants. The constant-roll inflation has novel dynamical features enriching physics, which is different from the slow-roll inflation. When the constant-roll inflation was proposed, it drawn widespread attention and was widely studied in lots of theories, such as  $f(R)$  gravity [20, 21],  $f(R, \phi)$  gravity [22],  $f(Q, T)$  gravity [23], scalar-tensor gravity [24], brane gravity [25], Dirac-Born-

Infeld theory [26], Galilean model [27], non-minimally coupled model [28, 29], non-minimally derivative coupling [30], quintessential model [31], holographic dark energy [32, 33], Tsallis holographic dark energy [34], and so on.

After inflation ended, the primordial inhomogeneities of the primordial power spectrum on small scales re-entered the Hubble horizon in the radiation dominated era, significant amount of primordial black holes (PBHs) can be formed as a result of the gravitational collapse [35, 36] if the amplitude of the primordial power spectrum produced during inflation is strong enough. After PBHs were proposed, they were found that they could be a candidate of dark matter [37] and were reconsidered [38, 39] after black holes mergers were detected by LIGO [40]. PBHs can offer us an opportunity to explore the physics of the early universe and may play some important roles in cosmology. Thus, PBHs were widely discussed in some modified gravity theories, such as scalar-tensor gravity [41],  $f(T)$  gravity [42], Brans-Dicke gravity [43],  $f(Q)$  gravity [44], teleparallel gravity [45],  $f(Q, T)$  gravity [23], and studied in some inflationary models including slow-roll inflation [46–66], ultra-slow-roll inflation [67–76] and constant-roll inflation [23, 77, 78]. PBHs also have attracted lots of attention since they may constitute part or all of dark matter [79–91], they may play a role in the synthesis of heavy elements [92–94] and could be responsible for some astrophysical phenomena, such as, seeding supermassive black holes [79, 84, 86, 95], seeding galaxies [79, 84], explaining the gravitational wave signals observed by the LIGO detectors [86, 96, 97]. The existence of PBHs formed in the early universe remains an open question. PBHs with masses smaller than  $5 \times 10^{14}g$  would have evaporated by Hawking radiation by now [98]. When PBHs are considered as dark matter, studies have suggested various possible mass ranges [82, 90, 99–101], though these proposals differ significantly in scale. Consequently, the allowed mass window for PBHs appears broad, but a more precise range requires further investigation. However, recent analyses have converged on the "asteroid mass" range of  $10^{17} - 10^{23}g$ , within which PBHs could potentially explain the entire dark matter [81, 102].

The holographic dark energy is one competitive candidate of dark energy [103–105], which is used to explain the late time acceleration of the universe, and is proposed based on the holographic principle stating that the entropy of a system is scaled on its surface area [106,

107]. The cornerstone of holographic dark energy is the horizon entropy, and different horizon entropy will result in different holographic dark energy models. Combining the holographic principle and Barrow entropy [108], Barrow holographic dark energy(BHDE) with different IR cutoff was proposed [109–113] and subsequently widely studied in theories [114–124] and observations [125–128]. Recently, the constant-roll inflation was studied in holographic dark energy model [32] and Tsallis holographic dark energy model [34], the results show that the constant-roll inflation can be realized in these models under some conditions. So, whether the constant-roll inflation consistent with observational constraints can be realized within the BHDE framework, and, if achievable, whether such a model can produce a sufficient abundance of primordial black holes.

This paper has two main objectives: to investigate constant-roll inflation and to explore the formation and evolution of PBHs in the framework of BHDE model. The paper is organized as follows: In Section II, we briefly review the modified Friedmann equation in BHDE model. In Section III, we investigate constant-roll inflation in BHDE model. In Section IV, we explore the formation and evolution of PBHs in BHDE model. Finally, our main conclusions are shown in Section V.

## II. MODIFIED FRIEDMANN EQUATIONS

In a homogeneous and isotropic Friedmann-Robertson-Walker universe described by the Friedmann-Lemaître-Robertson-Walker metric

$$ds^2 = -dt^2 + a(t)^2 \gamma_{ij} dx^i dx^j, \quad (1)$$

where  $a(t)$  denotes the scale factor, and  $\gamma_{ij}$  represents the metric on the three-sphere

$$\gamma_{ij} dx^i dx^j = \frac{dr^2}{1 - Kr^2} + r^2(d\theta^2 + \sin^2 \theta d\phi^2). \quad (2)$$

Here,  $K$  is the spatial curvature. Considering the apparent horizon as the IR cutoff, the Friedmann equation in BHDE model can be modified as [112]

$$\left(H^2 + \frac{K}{a^2}\right)^{1-\frac{\delta}{2}} = \frac{8\pi G_{eff}}{3} \rho_\phi, \quad (3)$$

where  $\delta$  satisfies the relation  $0 \leq \delta \leq 1$  and stands for the amount of the quantum-gravitational deformation effects [129],  $\delta = 0$  represents the standard holographic dark energy and  $\delta = 1$  denotes the most intricate and fractal structure of the horizon, and  $G_{eff}$  represents the effective Newtonian gravitational constant as

$$G_{eff} = \frac{A_0}{4} \left( \frac{2 - \delta}{2 + \delta} \right) \left( \frac{A_0}{4\pi} \right)^{\frac{\delta}{2}}. \quad (4)$$

In the case  $\delta \rightarrow 0$ , the area law of entropy is recovered, and we have  $A_0 \rightarrow 4G$ . As a result,  $G_{eff} \rightarrow G$  and the standard Friedmann equation is obtained.

We consider the matter contents of the early universe as a scalar field, and the energy density and the pressure take the form

$$\rho_\phi = \frac{1}{2} \dot{\phi}^2 + V(\phi), \quad p_\phi = \frac{1}{2} \dot{\phi}^2 - V(\phi), \quad (5)$$

which satisfies the continuity equation

$$\dot{\rho}_\phi + 3H(\rho_\phi + p_\phi) = 0. \quad (6)$$

It can be written as the Klein-Gordon equation

$$\ddot{\phi} + 3H\dot{\phi} + V_\phi = 0. \quad (7)$$

Combing Eqs. (3) and (6), the second Friedmann equation can be derived as [112]

$$(2 - \delta) \left( 1 + \frac{\dot{H}}{H^2} \right) \left( H^2 + \frac{K}{a^2} \right)^{-\frac{\delta}{2}} H^2 + (1 + \delta) \left( H^2 + \frac{K}{a^2} \right)^{1 - \frac{\delta}{2}} = -8\pi G_{eff} p_\phi. \quad (8)$$

### III. CONSTANT-ROLL INFLATION

In this section, we will discuss the constant-roll condition for the Friedmann equations given by Eqs. (3) and (8) in a flat universe. During inflation, the universe is characterized by the scalar spectral index parameter  $n_s$  and the tensor-to-scalar ratio  $r$  which are given by [130, 131]

$$n_s \simeq 1 - 4\epsilon_1 - 2\epsilon_2, \quad r = 16\epsilon_1, \quad (9)$$

with

$$\epsilon_1 = -\frac{\dot{H}}{H^2}, \quad \epsilon_2 = \frac{\ddot{\phi}}{H\dot{\phi}}. \quad (10)$$

For the slow-roll inflation,  $\epsilon_1 \ll 1$  and  $\epsilon_2 \ll 1$  are required. While in the constant-roll inflation, imposing  $\frac{\dot{\phi}^2}{2} < 1$ , only  $\epsilon_1 \ll 1$  is required to occur in the inflation, and the other constant-roll condition is given by

$$\ddot{\phi} = \gamma H \dot{\phi}. \quad (11)$$

Here,  $\gamma$  is a dimensionless real parameter. For  $\gamma = -3$ , the ultra slow-roll condition, which has a flat potential  $V_\phi = 0$ , is recovered. And the slow-roll condition is obtained for  $\gamma = 0$ . In the flat universe, considering  $\frac{\dot{\phi}^2}{2} < 1$ , Eqs. (3), (8) and (7) can be written as

$$H^2 \simeq \left( \frac{8\pi G_{eff}}{3} \right)^{\frac{2}{2-\delta}} V^{\frac{2}{2-\delta}}, \quad (12)$$

$$\dot{H} \simeq -\frac{3\dot{\phi}^2}{2(2-\delta)} \left( \frac{8\pi G_{eff}}{3} \right)^{\frac{2}{2-\delta}} V^{\frac{\delta}{2-\delta}}, \quad (13)$$

$$\dot{\phi} = -\frac{V_\phi}{(\gamma+3)H}. \quad (14)$$

Then, the constant-roll parameters become

$$\epsilon_1 = \frac{3\dot{\phi}^2}{2(2-\delta)V}, \quad \epsilon_2 = \gamma. \quad (15)$$

Similar to the slow-roll inflation occurring at the horizon crossing point, we also consider inflation begins at the horizon crossing point. Thus, the e-folds number  $N$ , which determines the amount of inflation, is given as

$$N = \int_{t_*}^{t_{end}} H dt, \quad (16)$$

where  $t_*$  and  $t_{end}$  represent the horizon crossing time and the end of inflation time, respectively. Rewriting the e-folds number  $N$  according to the scalar field, we obtain

$$N = \int_{\phi_*}^{\phi_{end}} \frac{H}{\dot{\phi}} d\phi. \quad (17)$$

To analyze the relation between the e-folds number  $N$  and the scalar spectral index parameter  $n_s$ , as well as the tensor-to-scalar ratio  $r$ , we consider five different inflation potentials.

### A. Power-law potential

We start with the simplest inflationary potential, the power-law potential, which takes the form

$$V = V_0 \phi^n, \quad (18)$$

according to the simplest chaotic inflationary models [132]. Here, both  $V_0$  and  $n$  are positive parameters. At the end of inflation, the first constant parameter  $\epsilon_1$  satisfies  $\epsilon_1(\phi_{end}) \simeq 1$  which gives

$$\phi_{end} = \left[ \left( \frac{8\pi G_{eff}}{3} \right)^{\frac{2}{2-\delta}} \frac{2(2-\delta)(\gamma+3)^2}{3n^2} V_0^{-\frac{\delta}{\delta-2}} \right]^{\frac{\delta-2}{4-2\delta+n\delta}}. \quad (19)$$

Here, Eqs. (12), (14) and (15) are taken into consideration. Then, the e-folds number can be written according  $\phi_{end}$  and  $\phi_*$

$$N = \left( \frac{8\pi G_{eff}}{3} \right)^{\frac{2}{2-\delta}} \frac{\gamma+3}{n} V_0^{-\frac{\delta}{2-\delta}} \frac{\delta-2}{4-2\delta+n\delta} \left( \phi_{end}^{-\frac{4-2\delta+n\delta}{\delta-2}} - \phi_*^{-\frac{4-2\delta+n\delta}{\delta-2}} \right). \quad (20)$$

Solving the above equation, we obtain the value of the scalar field at the horizon crossing  $\phi_*$

$$\phi_* = \left[ \left( \frac{8\pi G_{eff}}{3} \right)^{-\frac{2}{2-\delta}} V_0^{-\frac{\delta}{2-\delta}} \left( \frac{3n^2}{2(2-\delta)(\gamma+3)^2} - \frac{Nn}{\gamma+3} \frac{4-2\delta+n\delta}{\delta-2} \right) \right]^{-\frac{\delta-2}{4-2\delta+n\delta}}. \quad (21)$$

Using this result, the first constant-roll parameter  $\epsilon_1$  can be written as

$$\epsilon_1 = \frac{3n}{3n + 2(\gamma+3)[4 + (n-2)\delta]N}. \quad (22)$$

Then, the scalar spectral index parameter  $n_s$  and the tensor-to-scalar ratio  $r$  become

$$n_s = 1 - \frac{12n}{3n + 2(\gamma+3)[4 + (n-2)\delta]N} - 2\gamma, \quad (23)$$

$$r = \frac{48n}{3n + 2(\gamma+3)[4 + (n-2)\delta]N}, \quad (24)$$

which show that the parameters  $n_s$  and  $r$  depend on the power-term  $n$  of the chaotic potential, the constant-roll parameter  $\gamma$ , the parameter of the quantum-gravitational deformation effects  $\delta$  and the e-folds number  $N$ .

To determine the value of the power-term  $n$  in the power-law potential  $V = V_0 \phi^n$  and match our results with the observations, we adopt the constraints  $r_{0.002} < 0.058$  and  $n_s =$

$0.9668 \pm 0.0037$  from Planck TT,TE,EE + lowE + lensing + BK15 + BAO [133]. For model parameters, we consider  $\gamma$  in the range  $0.004 < \gamma < 0.018$ , while  $\delta$  is assigned a small value consistent with observational results [124–128]. To preserve the Big Bang Nucleosynthesis epoch,  $\delta$  must be within the bound  $\delta \leq 1.4 \times 10^{-4}$  [127], which provides the tightest constraint for  $\delta$ . Throughout this paper, we set  $\delta = 10^{-4}$ . Then, using Eqs. (23) and (24), we have plotted the prediction regions in  $\gamma - n$  plane with the number of e-folds  $N$  from 50 to 70 in Fig. (1). This figure shows that the value of  $\gamma$  is very small, and  $n$  is determined by  $\gamma$  and the e-folds number  $N$ .

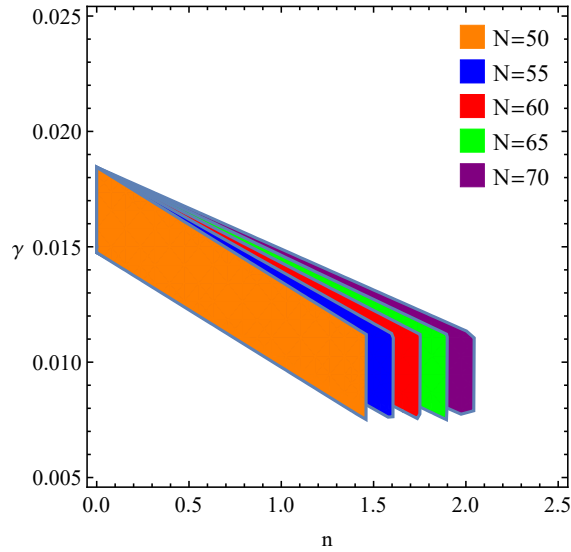


FIG. 1. Prediction regions in  $\gamma - n$  plane.

With the fixed value of  $n$ , we depict the predictions of the power-law potential (18) in  $r_{0.002} - n_s$  plane in Fig. (2) in which we overlap our analytical results with Planck 2018 data. These figures show that the value of  $r$  decreases as  $N$  varies from 50 to 70, and an increasing  $\gamma$  leads to a smaller value of  $n_s$ . It is obvious that the constant-roll parameter  $\gamma$  has an apparent influence on  $(r_{0.002}, n_s)$  behavior. With this comparison with the observation, the results show a good consistency for a specific range of the constant-roll parameter  $\gamma$  with Planck 2018 data, and the results prefer to the cases  $n \leq 1.1$ . It is evident that an increased value of  $n$  will lead to mismatch with the observations, and the value of  $\gamma$  is determined by



$n$  and increases as  $n$  decreases. For the case where  $n = 1$ ,  $\gamma$  takes the value 0.012. It is interesting to note that  $n = 1$  is also obtained in Tsallis holographic dark energy [34], and the power-law potential in slow-roll inflation within general relativity has been excluded by Planck 2018 data [7].

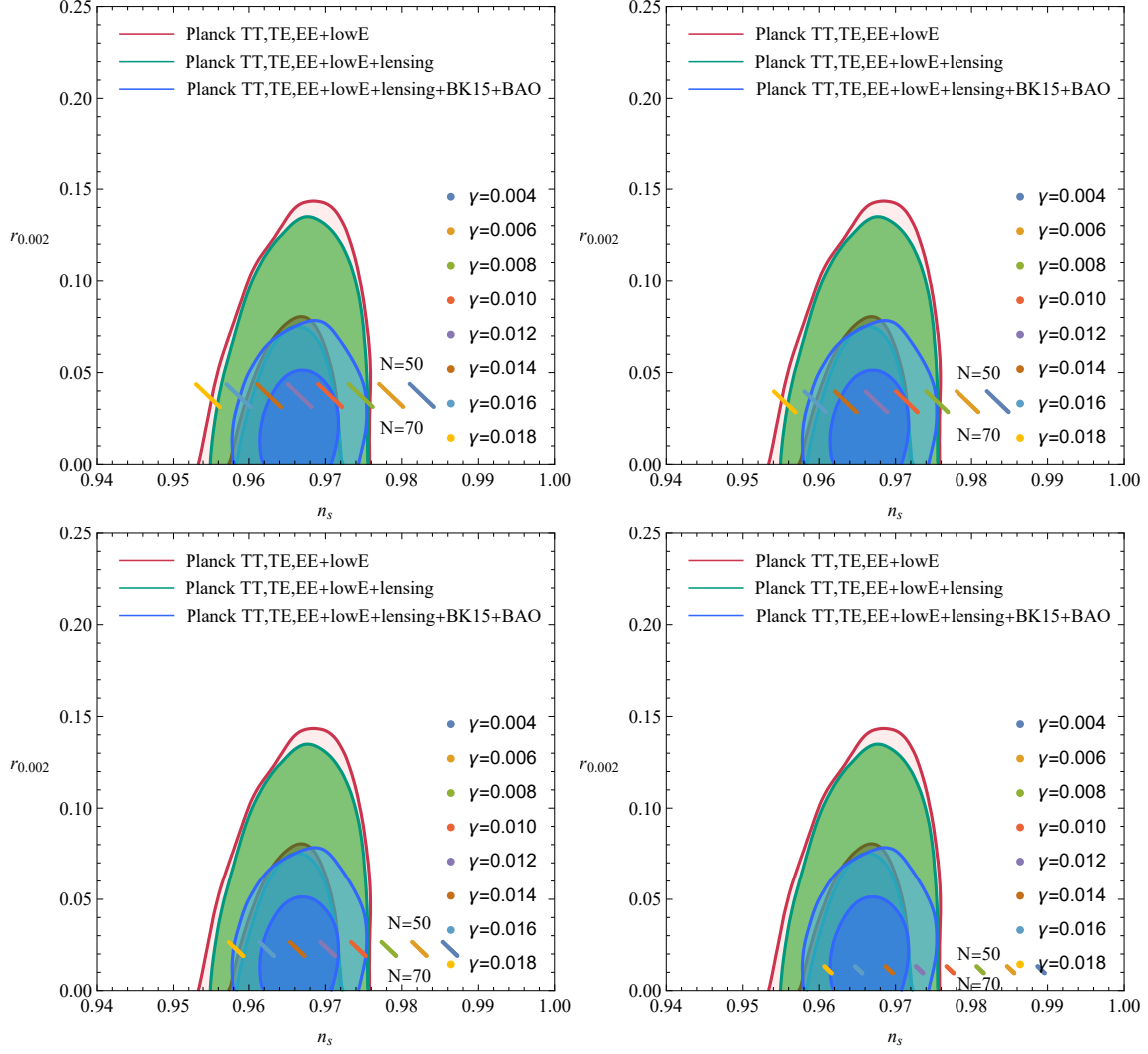


FIG. 2. Predictions of the power-law potential (18) in  $r_{0.002} - n_s$  plane. These panels are plotted for: (i)  $n = 1.1$ , (ii)  $n = 1$ , (iii)  $n = \frac{2}{3}$ , (iv)  $n = \frac{1}{3}$ .

## B. Periodic potential

The next potential we examine is the periodic potential

$$V = V_0 \left[ 1 + \cos \left( \frac{\phi}{f} \right) \right], \quad (25)$$

according to the natural inflation potential [134, 135]. Here,  $V_0$  and  $f$  are both positive parameters, where  $f$  controls the curvature of potential. Using the same analytical method as that in the previous subsection, we obtain the first constant-roll parameter  $\epsilon_1$  expressed as

$$\epsilon_1 \approx \frac{1}{2(2-\delta)} \frac{3^{\frac{\delta-4}{\delta-2}}}{(3+\gamma)^2 f^2} \frac{1}{e^{\frac{3N}{(3+\gamma)f^2}} \left[ 1 + \frac{9}{4(3+\gamma)^2 f^2} \right] - 1}. \quad (26)$$

Then, we can plot the prediction regions in  $\gamma - f$  plane with different e-folds number  $N$ , which is shown in Fig. (3). This figure demonstrates that  $\gamma$  takes a small value, and  $f$  is determined by the e-folds number  $N$ . With the increase of  $f$ , a large  $N$  is required.

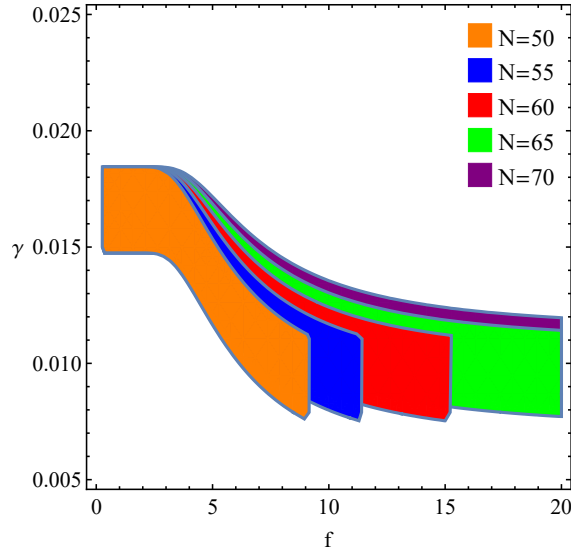


FIG. 3. Prediction regions in  $\gamma - f$  plane.

Then, fixing the value of  $f$ , we plot the predictions of the periodic potential (25) in  $r_{0.002} - n_s$  plane in Fig. (4) in which we overlap our analytical results with Planck 2018 data. Similar to the power-law potential, these figures also show that the value of  $r$  decreases as  $N$

varies from 50 to 70, and an increasing  $\gamma$  leads to a smaller value of  $n_s$ . By comparing with Planck 2018 data, the results show a good consistency for a specific range of the constant-roll parameter  $\gamma$  and the cases where  $f \leq 7$ . For the case where  $f = 7$ ,  $\gamma$  takes the value 0.012. These figures indicate that increasing  $f$  leads to mismatch with observations, and  $\gamma$  increases as  $f$  decreases. Additionally, the periodic potential in slow-roll inflation within general relativity is strongly disfavored by Planck 2018 data [7].

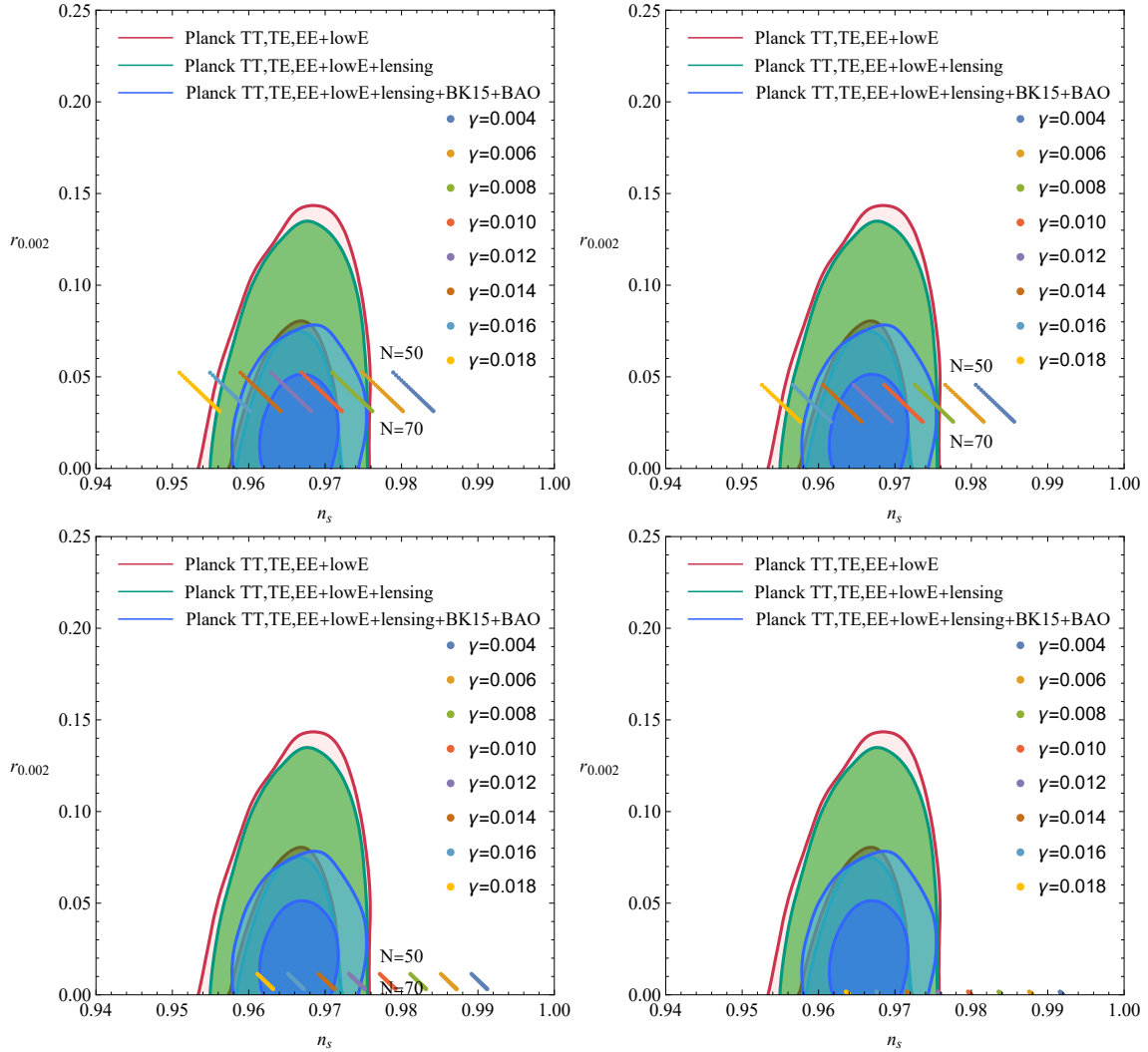


FIG. 4. Predictions of the periodic potential (25) in  $r_{0.002} - n_s$  plane. These panels are plotted for: (i)  $f = 8$ , (ii)  $f = 7$ , (iii)  $f = 4$ , (iv)  $f = 3$ .

### C. Hilltop potential

The last potential we analyze is the hilltop potential, which plays a significant role in inflationary cosmology and takes the form

$$V = V_0 \left[ 1 - \left( \frac{\phi}{\mu} \right)^p \right], \quad (27)$$

as defined in hilltop inflation [136]. Here,  $V_0$ ,  $\mu$ , and  $p$  are constant parameters of the model. Planck 2018 reported that the quartic potential provides a better fit than the quadratic potential, and  $\mu > 10$  is required in the quartic case [7]. To analyze the constant-roll inflation in the hilltop potential, we adopt the same analytical method as that in the previous subsections. However, due to the unique characteristics of hilltop potential and the computational complexity, we cannot obtain an analytical solution and need to employ numerical methods for complete analysis.

Fixing the values of  $p$  and  $\mu$ , we depict the predictions of the periodic potential (27) in  $r_{0.002} - n_s$  plane in Fig. (5) for some special cases. These figures also show that the value of  $r$  decreases as  $N$  varies from 50 to 70, and an increasing  $\gamma$  leads to a smaller value of  $n_s$ . To satisfy the observational constraints from Planck 2018 data,  $\mu$  must increase with the increase of  $p$ . As shown in these figures,  $p = 1$  requires  $\mu = 20$  while  $p = 4$  requires  $\mu = 150$  to satisfy these constraints. For all cases  $p = 1, 2, 3, 4$ , a consistent value of  $\gamma = 0.012$  is needed.

## IV. PRIMORDIAL BLACK HOLES

In the previous section, we have studied the constant-roll inflation in the BHDE model with power-law potential, periodic potential, and hilltop potential and found that they can be supported by the Planck 2018 data. During the radiation-dominated era after inflation, the enhanced primordial curvature perturbations at small scales may form PBHs through gravitational collapse when they re-enter the horizon. In standard slow-roll inflation, the PBHs formation probabilities remain exponentially suppressed because the curvature perturbation power spectrum fails to reach critical amplitude thresholds. In this section, we

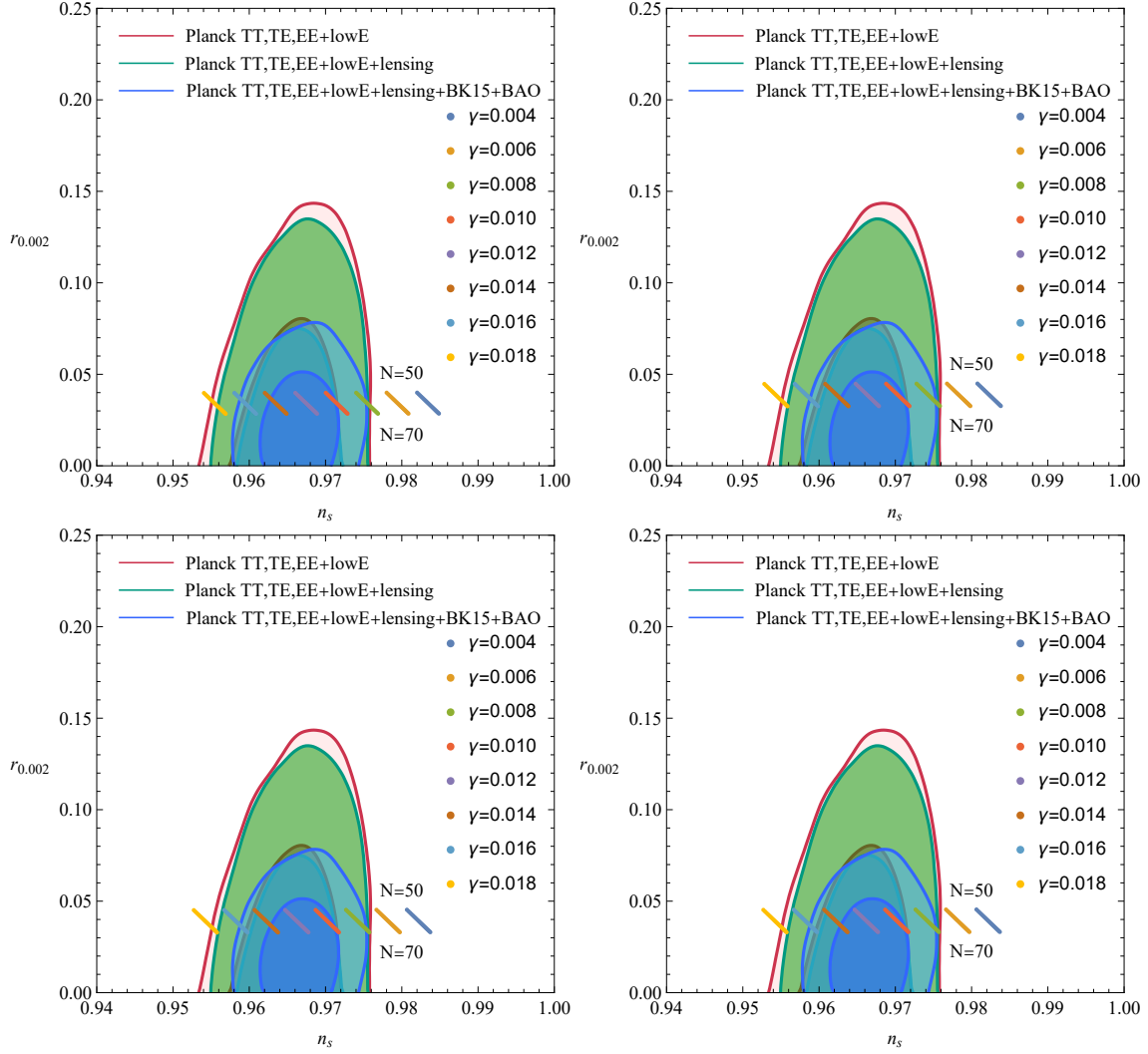


FIG. 5. Predictions of the hilltop potential (27) in  $r_{0.002} - n_s$  plane. These panels are plotted for: (i)  $p=1, \mu=20$ , (ii)  $p=2, \mu=50$ , (iii)  $p=3, \mu=100$ , (iv)  $p=4, \mu=150$ .

will discuss the formation and evolution of PBHs in the BHDE model.

## A. Formation

The mass of PBHs is related to the horizon mass when curvature perturbations with comoving wavenumber  $k$  reenter the cosmological horizon [137]

$$M(k) \simeq M_{\odot} \left( \frac{\gamma}{0.2} \right) \left( \frac{g_*}{10.75} \right)^{-\frac{1}{6}} \left( \frac{k}{1.9 \times 10^6 Mpc^{-1}} \right)^{-2}, \quad (28)$$

where  $M_{\odot}$  represents the Solar mass,  $\gamma \simeq (\frac{1}{\sqrt{3}})^3$  is the ratio of PBH mass to horizon mass and indicates the efficiency of collapse, and  $g_* = 106.75$  corresponds to the effective degrees of freedom in the energy density during the PBH formation. The production rate of PBHs with mass  $M(k)$  is given by [138, 139]

$$\beta(M) = \int_{\delta_c} \frac{d\delta}{\sqrt{2\pi\sigma^2(M)}} e^{-\frac{\delta^2}{2\sigma^2(M)}} = \frac{1}{2} \text{erfc}\left(\frac{\delta_c}{\sqrt{2\sigma^2(M)}}\right), \quad (29)$$

where  $\text{erfc}$  represents the complementary error function,  $\delta_c \simeq 0.4$  is the threshold of the density perturbations for the PBH formation [140, 141], and  $\sigma^2(M)$  denotes the variance of the coarse-grained density contrast, smoothed over the scale  $k$ , defined as [138]

$$\sigma^2(M(k)) = \frac{16}{81} \int \frac{dq}{q} W^2(q/k) (q/k)^4 \mathcal{P}_{\mathcal{R}}(q), \quad (30)$$

where  $W(x) = e^{-\frac{x^2}{2}}$  is the Gaussian window function, and  $\mathcal{P}_{\mathcal{R}}(k)$  is the power spectrum of the primordial curvature perturbations and takes the form

$$\mathcal{P}_{\mathcal{R}}(k) = \frac{k^3}{2\pi^2} \left| \frac{u_k}{z} \right|^2, \quad (31)$$

which can be solved from the Mukhanov-Sasaki equation

$$\ddot{u}_k + H\dot{u}_k + \left( \frac{c_s^2 k^2}{a^2} - \frac{\ddot{z} + H\dot{z}}{z} \right) u_k = 0, \quad (32)$$

with

$$z = \frac{a\dot{\phi}}{H}. \quad (33)$$

The current fractional energy density of PBHs with respect to the total dark matter density is given as [81]

$$\frac{\Omega_{PBH}}{\Omega_{DM}} = \int \frac{dM}{M} f(M) \quad (34)$$

with

$$f(M) = \frac{1}{\Omega_{DM}} \frac{d\Omega_{PBH}}{d \ln M} \simeq \frac{\beta(M)}{1.84 \times 10^{-8}} \left( \frac{\gamma}{0.2} \right)^{\frac{3}{2}} \left( \frac{10.75}{g_*} \right)^{\frac{1}{4}} \left( \frac{0.12}{\Omega_{DM} h^2} \right) \left( \frac{M}{M_\odot} \right)^{-\frac{1}{2}}. \quad (35)$$

Here, the value of  $\Omega_{DM} h^2$  is given by Planck 2018 data [133]. Based on the above equations, one can calculate PBH abundances and note that producing a sizable amount of PBHs requires the typical primordial curvature perturbations to be significant,  $\mathcal{P}_{\mathcal{R}} \sim O(10^{-2})$  on small scales. This value is about 7 orders of magnitude larger than the corresponding perturbations  $\mathcal{P}_{\mathcal{R}} \sim O(10^{-9})$  observed on Cosmic Microwave Background scales. To obtain enhanced primordial curvature perturbations at small scales, we consider that there is a small part with a periodic structure in the inflation potentials in the previous section, and the power-law potential (18), periodic potential (25), and hilltop potential (27) take the following form

$$V = V_0 \phi^n + \delta V, \quad (36)$$

$$V = V_0 \left[ 1 + \cos \left( \frac{\phi}{f} \right) \right] + \delta V, \quad (37)$$

$$V = V_0 \left[ 1 - \left( \frac{\phi}{\mu} \right)^p \right] + \delta V, \quad (38)$$

with

$$\delta V = \xi \sin \left( \frac{\phi}{\phi_*} \right) [1 + \tanh(10^6(\phi_e - \phi)(\phi - \phi_s))], \quad (39)$$

where  $\delta V$  represents a small periodic-structure contribution to the potential ( $\delta V \ll V$ ), with  $\xi$  quantifying the magnitude of the structure,  $\phi_*$  governing its characteristic period, and  $\phi_s$  and  $\phi_e$  specifying the starting and ending points of the structural feature respectively. This small periodic structure in the inflationary potential may amplify primordial curvature perturbations at small scales through parametric resonance mechanisms [142]. These enhanced primordial curvature perturbations could subsequently form observationally significant PBH populations upon horizon re-entry during the radiation-dominated era.

Choosing the potential parameters  $n = 1$ ,  $f = 7$ ,  $p = 1$ , and  $\mu = 20$  according to the results in the previous section, fixing the energy scale  $V_0 = 0.92 \times 10^{-10}$  and the period parameter  $\phi_* = 10^{-4}$ , and adopting the values of the structural parameters  $\xi$ ,  $\phi_s$ , and  $\phi_e$  listed in Tab. (I), we numerically solve the background equations (3), (7), and (8) and the

TABLE I. Model parameters and the numerical results.

<i>Potential</i>	$\xi(10^{-14})$	$\phi_e$	$\phi_s$	$N$	$n_s$	$r$	$k_{peak}(10^{12})$	$\mathcal{P}_{\mathcal{R}}^{peak}(10^{-12})$	$M_{peak}/M_{\odot}(10^{-12})$	$f_{PBH}^{peak}$	$\Omega_{PBH}/\Omega_{DM}$
<i>Power – law</i>	35.367	8.30	8.35	59.99	0.9676	0.0335	1.704	0.473	1.40	0.979	0.334
<i>Periodic</i>	5.450	10.79	10.84	59.97	0.9676	0.0336	1.917	0.262	1.10	0.982	0.337
<i>Hilltop</i>	1.7792	11.70	11.75	59.98	0.9676	0.0338	1.857	0.493	1.60	0.981	0.331

perturbation equation (32) in the flat universe under the constant-inflation condition (11) to obtain the scalar power spectrum, as shown in the left panel of Fig. (6). In this figure, we overlap our numerical results with the observational data from CMB [133],  $\mu$ -distortion [143], BBN [144], and EPTA [145]. For the power-law, periodic, and hilltop potential models, the numerical results of the e-folds number  $N$ , the scalar spectral index parameter  $n_s$ , the tensor-to-scalar ratio  $r$ , the peak scales  $k_{peak}$ , and the peak values of the primordial curvature perturbation power spectrum  $\mathcal{P}_{\mathcal{R}}^{peak}$  are shown in Tab. (I). It can be seen that the numerical results of the primordial curvature perturbation power spectra not only satisfy the current observational constraints but also achieve a peak amplitude of the order of  $10^{-2}$  at small scales. This enhancement indicates that these models can generate a sufficient number of PBHs, providing theoretical support for PBH formation.

Then, combining the numerical results of the primordial curvature perturbation power spectra in the left panel of Fig. (6) with Eqs. (28), (29), (30), (34), and (35), we obtain the peak masses of PBHs  $M_{peak}$ , the PBHs abundance  $f_{PBH}$ , and the current fraction of PBHs in dark matter density  $\Omega_{PBH}/\Omega_{DE}$ , as shown in the right panel of Fig. (6) and Tab. (I). In the right panel of Fig. (6), we overlap our numerical results with observational data from EG $\gamma$  [146], WD [147], INTEGRAL [148], Kepler [149], Subaru HSC [150], EROS/MACHO [151], and CMB [152]. The detailed numerical results for the power-law, periodic, and hilltop potential models in Tab. (I) show that PBHs with a mass of approximately  $10^{-12}M_{\odot}$  exhibit a peak abundance  $f_{PBH}^{peak}$  exceeding 0.97 and approaching 1. These results indicate that a sufficient number of PBHs can form and are consistent with current observational limit. Since the corresponding density ratio  $\Omega_{PBH}/\Omega_{DE}$  is approximately 0.33, PBHs can account for one-third of the dark matter.



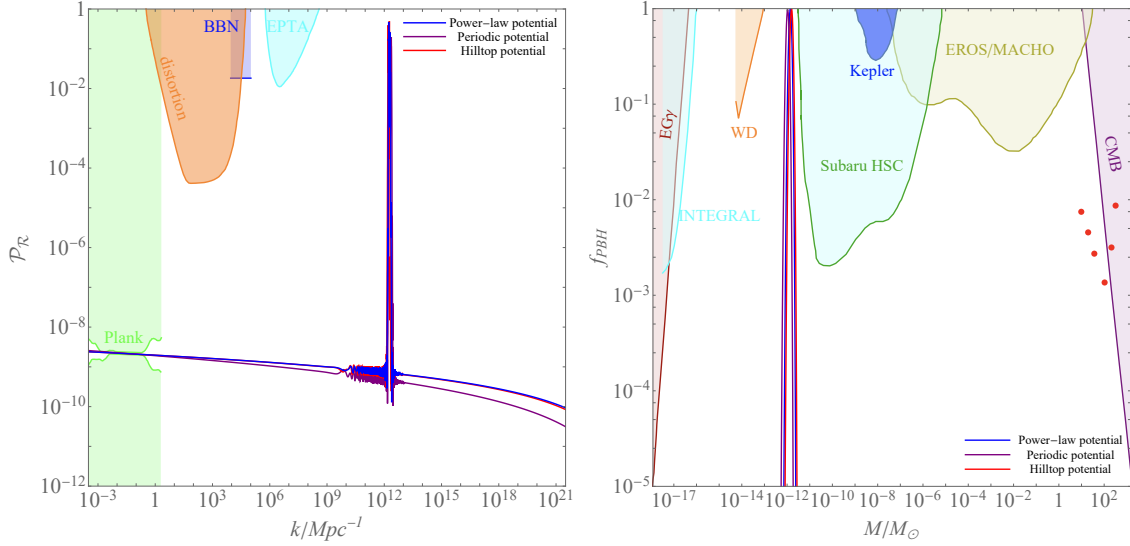


FIG. 6. Results for the primordial curvature perturbation power spectrum  $\mathcal{P}_{\mathcal{R}}$  and PBHs abundances  $f_{PBH}$ .

## B. Evolution

In the previous subsection, we analyzed the formation of PBHs in constant-roll inflation under the BHDE model and found that the mass of the formed PBHs is nearly  $10^{-12}M_{\odot}$ . In this subsection, we examine the evolution of PBHs assuming their formation occurred during the radiation-dominated era within the BHDE framework. The black holes (BHs) can evolve with an increasing mass by absorbing other matter, stars and BHs. During this process, BHs can emit particles. The quantum properties of BHs show that the possibility of emitting particles with a thermal spectrum is related to BHs' surface gravity [153]. During the process of emitting particles, BHs may lose mass. In the following, we will analyze the thermal properties of evaporating PBHs. The corresponding PBHs temperatures are given as [153, 154]

$$T_{PBH} = \frac{\hbar c^3}{8\pi G M_{PBH} k} \sim 1.06 \left( \frac{10^{10}}{M_{PBH}} \right) GeV, \quad (40)$$

where  $M_{PBH}$  is the total mass of PBHs.

To discuss the evaporation mass of PBHs, we consider the main process to decrease the mass of PBHs is Hawking evaporation, which is defined as [155, 156]

$$\left(\frac{dM}{dt}\right)_{eva} = -\frac{\hbar c^4}{G^2} \frac{\alpha_s}{M^2}, \quad (41)$$

where  $\alpha_s$  is the spin parameter of the emitting particle. Integrating Eq. (41), the evaporation mass of PBHs is obtained

$$M_{eva} = M_i \left(1 - \frac{t}{t_{eva}}\right)^{\frac{1}{3}}, \quad (42)$$

with

$$t_{eva} = \frac{G^2}{\hbar c^4} \frac{M_i^3}{3\alpha_s}, \quad (43)$$

where  $M_i$  is the initial mass of PBHs and  $t_{eva}$  denotes the Hawking evaporation time scale. The initial mass of PBHs is given as the order of the particle horizon mass when it was formed [157]

$$M_i \approx \frac{c^3 t_f}{G} \approx \frac{10^{12} t_f}{10^{-23}}. \quad (44)$$

Here,  $t_f$  is the time of its formation. So, the PBHs formed in the late time of the universe must have more mass than that formed in the early time. For the case of PHBs formed at Planck time  $10^{-43}s$ , it had the mass  $10^{-8}kg$ . For an initial mass  $M_i = 2 \times 10^{30}kg$ , which is the mass of sun  $M_\odot$ , it requires  $t_f = 2 \times 10^{-5}s$ . For  $M_i = 1.1 \times 10^{-12}M_\odot$ , which is the peak masse of PBHs obtained in previous subsection, it requires  $t_f = 2.2 \times 10^{-17}s$ .

Eq. (42) shows the evolution of the evaporation mass of PBHs with respect to  $t/t_{eva}$ . The evaporation mass decreasing as  $t$  approaches to  $t_{eva}$  and becomes 0 for  $t = t_{eva}$ , which indicates PBHs evaporate completely. The evolution of  $M_{eva}/M_i$  as the functions of  $t/t_{eva}$  is plotted in the left panel of Fig. (7), which is also given in Ref. [23]. So, the Hawking evaporation time scale  $t_{eva}$  determines the evaporation time of PBHs. According to Eq. (43), we can find that  $t_{eva}$  increases with the increase of  $M_i$  and decreases with the increase of  $\alpha_s$ . In the right panel of Fig. (7), by considering the evaporation time  $t_{eva}$  as a function of the initial mass of PBHs  $M_i$ , we have plotted the relation between  $t_{eva}$  and  $M_i$ . The red dashed line in this figure represents the current age of the universe. This figure shows that the PBHs need more time to achieve a complete evaporation with the increase of the initial mass, and it needs a evaporation time longer than the age of the universe when the initial

mass is larger than  $5 \times 10^{11} kg$ , which is shown in Ref. [98]. For  $\alpha_s \sim 10^{-4}$  [155, 157], we can write  $t_{eva}$  as

$$t_{eva} \sim 10^{-17} M_i^3. \quad (45)$$

For the initial mass equal to the peak mass of PBHs  $M_i = 1.1 \times 10^{-12} M_\odot = 2.2 \times 10^{18} kg$ , the evaporation time  $t_{eva}$  is nearly  $10^{38} s$ , which is much larger than the age of the universe. So, in these models, PBHs have not evaporated completely at the present time.

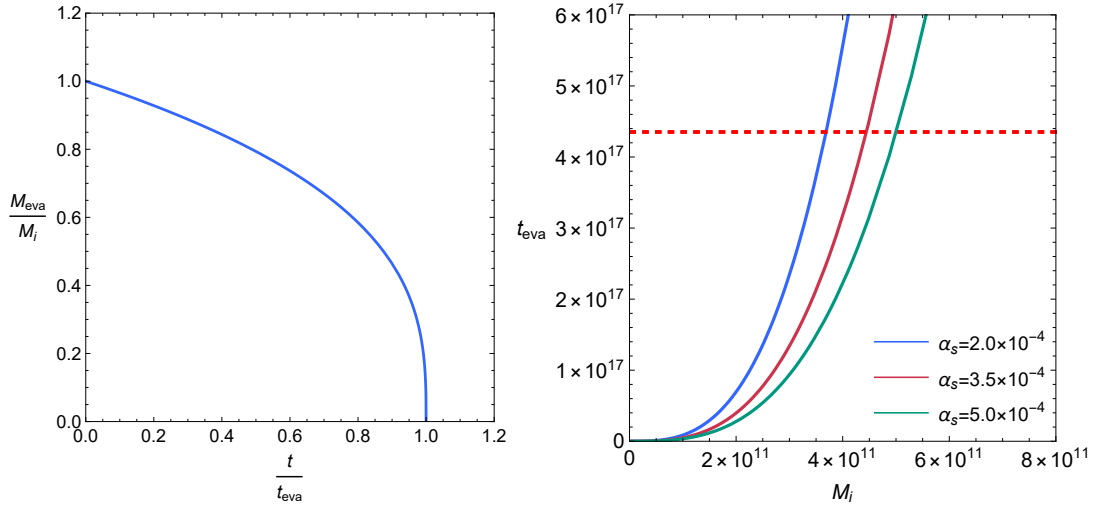


FIG. 7. The evolution of  $M_{eva}/M_i$  as a function of  $t/t_{eva}$  is plotted in the left panel, and the relation between the initial mass of PBHs  $M_i$  and the evaporation time  $t_{eva}$  is shown in the right panel. The red dashed line denotes the age of the universe.

During the process of evaporation, the accretion of fluid surrounding PBHs will prolong the evaporation of PBHs. So, we require to consider the process of the mass accretion rate for PBHs with fluid, which is given as [157, 158]

$$\left(\frac{dM}{dt}\right)_{accr} = \frac{16\pi G^2}{c^3} M^2 (\rho_{eff} + p_{eff}). \quad (46)$$

Here,  $\rho_{eff}$  and  $p_{eff}$  represent the effective energy density and pressure, respectively. Using Eqs. (3) and (8), we can obtain

$$\rho_{eff} = \frac{3}{8\pi G} H^2, \quad \omega_{eff} = \frac{p_{eff}}{\rho_{eff}} = \frac{2\omega_\phi + \delta}{2 - \delta}, \quad (47)$$

in which  $\omega_\phi = p_\phi/\rho_\phi$ . When  $\delta$  takes a small value, one can obtain  $\omega_{eff} \approx \omega_\phi$ . Considering  $a \sim t^{\frac{2}{3(1+\omega_{eff})}}$  and  $H = \frac{2}{3(1+\omega_{eff}t)}$ , we can write  $\rho_{eff} + p_{eff}$  as

$$\rho_{eff} + p_{eff} = \frac{1}{6\pi G(1 + \omega_{eff})t^2}. \quad (48)$$

Here, we consider that  $\rho_{eff} + p_{eff}$  evolves with  $t$  instead of a constant in Ref. [23]. Then, Eq. (46) can be integrated as

$$M_{accr} = \frac{M_i}{1 - \beta\left(1 - \frac{t_i}{t}\right)} \quad (49)$$

with

$$\beta = \frac{8G}{3c^2(1 + \omega_{eff})} \frac{M_i}{t_i}, \quad (50)$$

in which  $t_i$  is the time that PBHs begins to accrete,  $\beta$  denotes the product of the accretion efficiency and the fraction of the horizon mass [159]. Assuming PBHs begins to accrete at the time when it formed, we obtain  $t_i = t_f$ . Then, using Eq. (44),  $\beta$  and  $t_i/t$  can be written as

$$\beta \approx \frac{0.6588}{1 + \omega_{eff}}, \quad (51)$$

which indicates  $\beta$  is only determined by  $\omega_{eff}$  and decreases with the increase of  $\omega_{eff}$ , and

$$\frac{t_i}{t} = \frac{10^{-35}M_i}{t}, \quad (52)$$

which equals to 1 at the time PBHs begins to accrete and decays very fast. So, according to Eq. (49), we can obtain  $M_{accr} \simeq M_i$  at the initial time  $t_i$ . The evolution curve of  $\beta$  and  $t_i/t$  are plotted in the left and right panel of Fig. (8) respectively. In the left panel of Fig. (9), we have plotted the evolutionary curves for  $M_{accr}/M_i$  as the function of  $t$ . This figure shows that  $M_{accr}/M_i$  increases with the decrease of  $\omega_{eff}$ , and it increases rapidly in a short time and then keeps as a constant. The right panel of Fig. (9) shows the relation between  $M_{accr}/M_i$  and  $\omega_{eff}$ . From these figures, we can see that  $M_{accr}/M_i$  increases to approach  $10^2$  when  $\omega_{eff}$  decreases from  $1/3$  to  $-1/3$ .

Considering PBHs begin to accrete and evaporate after their formation, we plot the evolutionary curves of PBH mass  $M_{PBH}$  and temperature  $T_{PBH}$  in Fig. (10). The left panel of Fig. (10) shows the evolutionary curves of PBHs mass  $M_{PBH}$  as the function of  $t$ . From

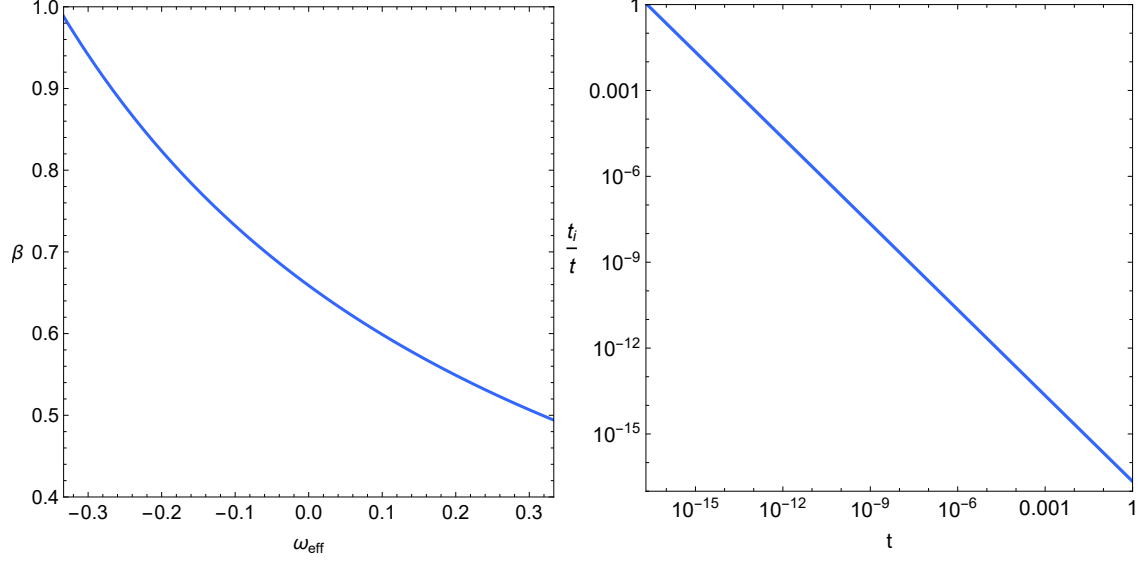


FIG. 8. The evolution of  $\beta$  as a function of  $\omega_{\text{eff}}$  is plotted in the left panel, and that of  $t_i/t$  as a function of  $t$  is plotted in the right panel. The initial mass of PBHs takes the value  $M_i = 1.1 \times 10^{-12} M_\odot$ .

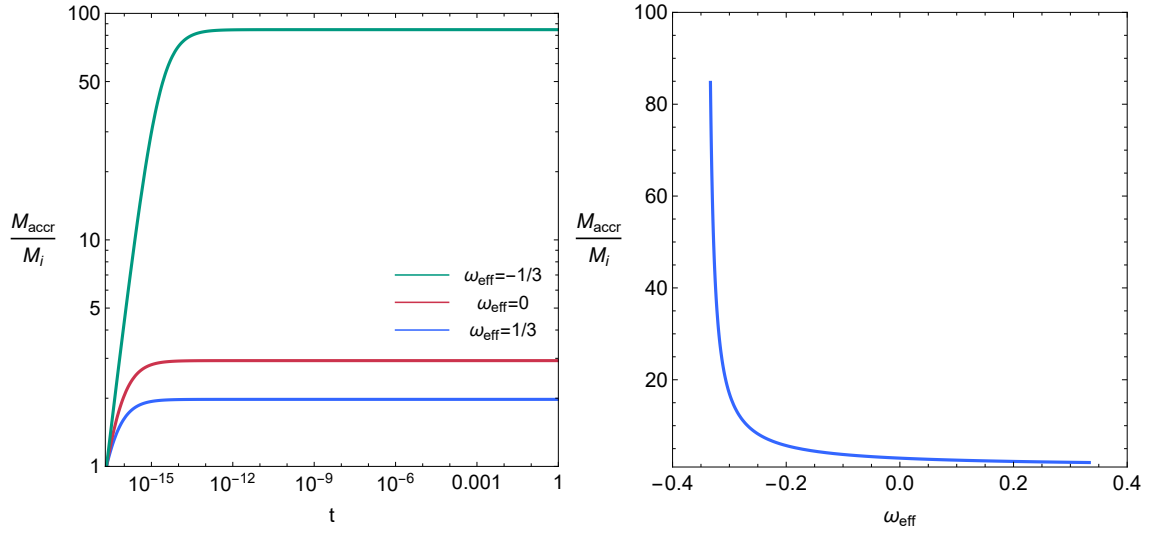


FIG. 9. Evolutionary curves of  $M_{\text{accr}}/M_i$ . The left panel sets  $t$  as the variable, while the right panel sets  $\omega_{\text{eff}}$ . The initial mass of PBHs takes the value  $M_i = 1.1 \times 10^{-12} M_\odot$ .

this figure, we can see that  $M_{PBH}$  increases rapidly in a short time and then keeps as a constant, and  $M_{PBH}$  increases with the decrease of  $\omega_{eff}$ . In the right panel of Fig. (10), we have plotted the evolutionary curves of PBHs temperature  $T_{PBH}$  as the function of  $t$ . Since  $T_{PBH}$  is inversely proportional to  $M_{PBH}$ , which is given in Eq. (40),  $T_{PBH}$  decreases rapidly in a very short time and then becomes a constant, and  $T_{PBH}$  decreases with the decrease of  $\omega_{eff}$ . When  $\omega_{eff}$  evolves from  $1/3$  to  $-1/3$ , the PBHs temperature  $T_{PBH}$  decreases from  $10^{-9}GeV$  to  $10^{-11}GeV$ , i.e.  $T_{PBH}$  decreases from  $10^4K$  to  $10^2K$ . These results indicate that PBHs still exist and can be detected today, but they persist at relatively low temperatures.

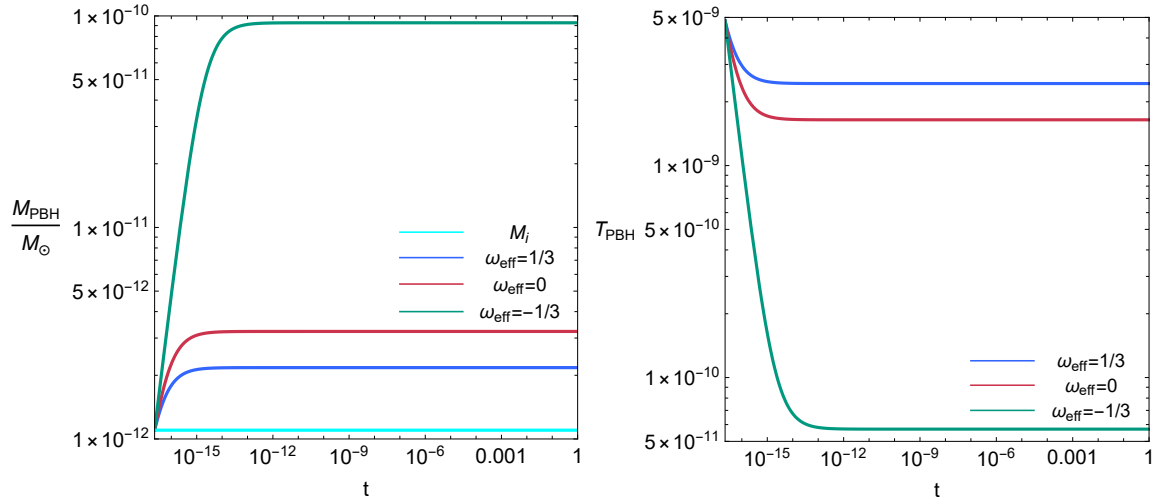


FIG. 10. Evolutionary curves of PBH mass  $M_{PBH}$  and PBH temperature  $T_{PBH}$ . The initial mass of PBHs takes the value  $M_i = 1.1 \times 10^{-12} M_\odot$ .

After inflation ended and PHBs formed, the universe evolves from the radiation dominated epoch to the pressureless matter dominated epoch, and then enters into the dark energy dominated epoch, the effective equation of state parameter evolves from  $1/3$  to less than  $-1/3$ , the accretion mass  $M_{accr}$  increases to approach  $10^2 M_i$ , the PBHs temperature  $T_{PBH}$  decreases with the increase of  $M_{PBH}$ .

## V. CONCLUSION

Based on the holographic principle and Barrow entropy, a new BHDE model with the apparent horizon as an IR cutoff has been proposed, and the corresponding Friedmann equation has been modified. In this paper, using the modified Friedmann equation and the constant-roll condition, we calculate the constant-roll parameters  $\epsilon_1$  and  $\epsilon_2$ , the scalar spectral index parameter  $n_s$ , and the tensor-to-scalar ratio  $r$  for the power-law, periodic, and hilltop potential models. By applying the Planck 2018 data, we plot the  $r_{0.002} - n_s$  plane to obtain suitable values for the model parameters by considering  $\delta = 10^{-4}$ . For the power-law potential model, results indicate an upper bound of  $n \leq 1.1$ ; for the periodic potential model, observed data constrain  $f \leq 7$ ; for the hilltop potential model, the preferred parameter range limits  $p \leq 4$ .

Then, we analyze the formation and evolution of PBHs in the BHDE model, which formed during the radiation-dominated era following the end of inflation. By considering the results of constant-roll inflation and the parametric resonance mechanisms for the power-law, periodic, and hilltop potential models, we calculate the primordial curvature perturbation power spectra of these models and obtain a peak amplitude of the order of  $10^{-2}$  at small scales. Based on these spectra, we investigate the abundance of PBHs and obtain the PBH mass approximately as  $10^{-12}M_\odot$  with a peak abundance  $f_{PBH}^{peak} > 0.97$  and the corresponding density ratio  $\Omega_{PBH}/\Omega_{DE}$  is approximately 0.33. These results indicate that such models both generate sufficient PBHs and account for approximately one-third of the dark matter content. Subsequently, by analyzing the evolution of the evaporation mass  $M_{eva}$  and the accretion mass  $M_{accr}$  of PBHs with the initial mass  $M_i = 10^{-12}M_\odot$  when the effective equation of state parameter  $\omega_{eff}$  evolves from  $1/3$  to  $-1/3$ , we find the accretion mass  $M_{accr}$  increases to approximately  $10^2 M_i$ , while the temperature of PBHs  $T_{PBH}$  decreases from  $10^4 K$  to  $10^2 K$ . These results indicate that PBHs still exist and can be detected today, but they persist at relatively low temperatures.

## ACKNOWLEDGMENTS

This work was supported by the National Natural Science Foundation of China under Grants Nos.12405081, 12265019, 11865018, 12305056, 11505004.

---

- [1] A. Guth, Phys. Rev. D **23**, 347 (1981).
- [2] A. Linde, Phys. Lett. B **108**, 389 (1982).
- [3] V. Mukhanov, G. Chibisov, JETP Lett. **33**, 532 (1981).
- [4] A. Lewis, A. Challinor, A. Lasenby, Astrophys. J. **538**, 473 (2000).
- [5] F. Bernardeau, S. Colombi, E. Gaztanaga, R. Scoccimarro, Phys. Rep. **367**, 1 (2002).
- [6] S. Weinberg, Cosmology, Oxford Univ. Press (2008).
- [7] Planck Collaboration, A&A **641**, A10 (2020).
- [8] M. Maggiore, Gravitational Waves, Oxford Univ. Press (2018).
- [9] H. Noh and J. Hwang, Phys. Lett. B **515**, 231 (2001).
- [10] J. Martin, H. Motohashi, T. Suyama, Phys. Rev. D **87**, 023514 (2013).
- [11] K. Dimopoulos, Ultra slow-roll inflation demystified. Phys. Lett. B **775**, 262 (2017).
- [12] C. Pattison, V. Vennin, H. Assadullahi, and D. Wands, JCAP **08**, 048 (2018).
- [13] H. Motohashi, A. Starobinsky, J. Yokoyama, JCAP **09**, 018 (2015).
- [14] Q. Gao, Sci. China Phys. Mech. Astron. **60**, 090411 (2017).
- [15] Q. Gao, Sci. China Phys. Mech. Astron. **61**, 070411 (2018).
- [16] Z. Yi, Y. Gong, JCAP **03**, 052 (2018).
- [17] L. Anguelova, P. Suranyi, L.C.R. Wijewardhana, JCAP **02**, 004 (2018).
- [18] F. Ciccirella, J. Mabillard, M. Pieroni, JCAP **01**, 024 (2018).
- [19] M. Guerrero, D. Rubiera-Garcia, D. Gomez, Phys. Rev. D **102**, 123528 (2020).
- [20] S. Nojiri, S. Odintsov, and V. Oikonomou, Class. Quantum Grav. **34**, 245012 (2017).
- [21] H. Motohashi, A. Starobinsky, Eur. Phys. J. C **77**, 538 (2017).
- [22] S. Panda, A. Rana, and R. Thakur, Eur. Phys. J. C **83**, 297 (2023).



- [23] K. Bourakadi, M. Koussour, G. Otalora, M. Bennai, and T. Ouali, *Phys. Dark Univ.* **41**, 101246 (2023).
- [24] H. Motohashi and A. Starobinsky, *JCAP* **11**, 025 (2019).
- [25] A. Mohammadi, T. Golanbari, S. Nasri, and K. Saaidi, *Phys. Rev. D* **101**, 123537 (2020).
- [26] S. Lahiri, *Mode. Phys. Lett. A* **37**, 2250003 (2022).
- [27] R. Herrera, M. Shokri, and J. Sadeghi, *Phys. Dark Univ.* **41**, 101232 (2023).
- [28] A. Karam, L. Marzola, T. Pappas, A. Racioppi, and K. Tamvakis, *JCAP* **05**, 011 (2018).
- [29] M. Shokri, J. Sadeghi, M. Setare, and S. Capozziello, *Int. J. Mode. Phys. D* **30**, 2150070 (2021).
- [30] J. Liu, Y. Gong, Z. Yi, *Commun. Theor. Phys.* **76** 095401 (2024).
- [31] M. Shokri, J. Sadeghi, S. Gashti, *Phys. Dark Univ.* **35** 100923 (2022).
- [32] A. Mohammadi, *Phys. Dark Univ.* **36**, 101055 (2022).
- [33] S. Nojiri, S. Odintsov, and T. Paul, *Phys. Lett. B* **841**, 137926 (2023).
- [34] A. Keskin and K. Kurt, *Eur. Phys. J. C* **83**, 72 (2023).
- [35] S. Hawking, *Mon. Not. Roy. Astron. Soc.* **152**, 75 (1971).
- [36] B. Carr and S. Hawking, *Mon. Not. Roy. Astron. Soc.* **168**, 399 (1974).
- [37] G. Chapline, *Nature* **253**, 251 (1975).
- [38] S. Bird, I. Cholis, J. Munoz, Y. Ali-Haïmoud, M. Kamionkowski, E. Kovetz, A. Raccanelli, and A. Riess, *Phys. Rev. Lett.* **116**, 201301 (2016).
- [39] M. Sasaki, T. Suyama, T. Tanaka, and S. Yokoyama, *Phys. Rev. Lett.* **117**, 061101 (2016).
- [40] B. Abbott *et al.* (LIGO Scientific Collaboration and Virgo Collaboration), *Phys. Rev. D* **93**, 122003 (2016).
- [41] J. Barrow and B. Carr, *Phys. Rev. D* **54**, 3920 (1996).
- [42] J. Bhadra and U. Debnath, *Int. J. Theor. Phys.* **53**, 645 (2013).
- [43] G. Aliferis and V. Zarikas, *Phys. Rev. D* **103**, 023509 (2021).
- [44] A. Chanda and B. Paul, *Eur. Phys. J. C* **82**, 616 (2022).
- [45] K. Bourakadi, B. Asfour, Z. Sakhi, M. Bennai, and T. Ouali, *Eur. Phys. J. C* **82**, 792 (2022).
- [46] B. Carr and J. Lidsey, *Phys. Rev. D* **48**, 543 (1993).

- [47] P. Ivanov, P. Naselsky, and I. Novikov, Phys. Rev. D **50**, 7173 (1994).
- [48] J. Yokoyama, Phys. Rev. D **58**, 083510 (1998).
- [49] J. Garcia-Bellido and E. Ruiz Morales, Phys. Dark Univ. **18**, 47 (2017).
- [50] S. Pi, Y. Zhang, Q. Huang, and M. Sasaki, JCAP **05**, 042 (2018).
- [51] M. Biagetti, G. Franciolini, A. Kehagias, and A. Riotto, JCAP **07**, 032 (2018).
- [52] C. Fu, P. Wu, and H. Yu, Phys. Rev. D **102**, 043527 (2020).
- [53] M. Davies, P. Carrilho, and D. Mulryne, JCAP **06**, 019 (2022).
- [54] J. Lin, Q. Gao, Y. Gong, Y. Lu, C. Zhang, and F. Zhang, Phys. Rev. D **101**, 103515 (2020).
- [55] Z. Yi, Q. Gao, Y. Gong, and Z. Zhu, Phys. Rev. D **103**, 063534 (2021).
- [56] Q. Gao, Y. Gong, and Z. Yi, Nucl. Phys. B **969**, 115480 (2021).
- [57] Q. Gao, Sci. China Phys. Mech. Astron. **64**, 280411 (2021).
- [58] Z. Yi, Y. Gong, B. Wang, and Z. Zhu, Phys. Rev. D **103**, 063535 (2021).
- [59] L. Wu, Y. Gong, and T. Li, Phys. Rev. D **104**, 123544 (2021).
- [60] Z. Wang, S. Gao, Y. Gong, and Y. Wang, Phys. Rev. D **109**, 103532 (2024).
- [61] X. Wang, Y. Zhang, and M. Sasaki, JCAP **07**, 076 (2024).
- [62] L. Chen, H. Yu, and P. Wu, Phys. Lett. B **849**, 138457 (2024).
- [63] M. Solbi and K. Karami, Eur. Phys. J. C **84**, 918 (2024).
- [64] D. Frolovsky and S. Ketov, Phys. Rev. D **111**, 083533 (2025).
- [65] A. Afzal, A. Ghoshal, and S. King, Phys. Rev. D **111**, 023050 (2025).
- [66] S. Choudhury, A. Karde, P. Padiyar, and M. Sami, Eur. Phys. J. C **85**, 21 (2025).
- [67] H. Di and Y. Gong, JCAP **07**, 007 (2018).
- [68] C. Fu, P. Wu, and H. Yu, Phys. Rev. D **100**, 063532 (2019).
- [69] G. Ballesteros, J. Rey, M. Taoso, and A. Urbano, JCAP **08**, 043 (2020).
- [70] Y. Liu, Q. Wang, B. Su, and N. Li, Phys. Dark Univ. **34**, 100905 (2021).
- [71] D. Figueroa, S. Raatikainen, S. Rasanen, and E. Tomberg, JCAP **05**, 027 (2022).
- [72] R. Zhai, H. Yu, and P. Wu, Phys. Rev. D **106**, 023517 (2022).
- [73] L. Chen, H. Yu, and P. Wu, Phys. Rev. D **106**, 063537 (2022).
- [74] R. Zhai, H. Yu, and P. Wu, Phys. Rev. D **108**, 043529 (2023).

- [75] S. Choudhury, A. Karde, S. Panda, and S. SenGupta, *Eur. Phys. J. C* **84**, 1149 (2024).
- [76] B. Su, N. Li, and L. Feng, *Eur. Phys. J. C* **85**, 197 (2025).
- [77] H. Motohashi, S. Mukohyama, and M. Oliosi, *JCAP* **03**, 002 (2020).
- [78] E. Tomberg, *Phys. Rev. D* **108**, 043502 (2023).
- [79] S. Clesse and J. Garcia-Bellido, *Phys. Rev. D* **92**, 023524 (2015).
- [80] M. Kawasaki, A. Kusenko, Y. Tada, and T. T. Yanagida, *Phys. Rev. D* **94**, 083523 (2016).
- [81] B. Carr, F. Kuhnel, and M. Sandstad, *Phys. Rev. D* **94**, 083504 (2016).
- [82] K. Inomata, M. Kawasaki, K. Mukaida, Y. Tada, and T. Yanagida, *Phys. Rev. D* **96**, 043504 (2017).
- [83] K. Inomata, M. Kawasaki, K. Mukaida, and T. Yanagida, *Phys. Rev. D* **97**, 043514 (2018).
- [84] B. Carr and J. Silk, *Mon. Not. Roy. Astron. Soc.* **478**, 3756 (2018).
- [85] C. Germani and I. Musco, *Phys. Rev. Lett.* **122**, 141302 (2019).
- [86] A. Kusenko, M. Sasaki, S. Sugiyama, M. Takada, V. Takhistov, and E. Vitagliano, *Phys. Rev. Lett.* **125**, 181304 (2020).
- [87] R. Calabrese, D. Fiorillo, G. Miele, S. Morisi, and A. Palazzo, *Phys. Lett. B* **829**, 137050 (2022).
- [88] J. de Freitas Pacheco, E. Kiritsis, M. Lucca, and J. Silk, *Phys. Rev. D* **107**, 123525 (2023).
- [89] M. Flores and A. Kusenko, *JCAP* **05**, 013 (2023).
- [90] V. Dike, D. Gilman, T. Treu, *Mon. Not. Roy. Astron. Soc.* **522**, 5434 (2023).
- [91] J. de Freitas Pacheco and J. Silk, *Phys. Rev. D* **101**, 083022 (2020).
- [92] M. Calza, D. Pedrotti, and S. Vagnozzi, *Phys. Rev. D* **111**, 024010 (2025).
- [93] G. Fuller, A. Kusenko, and V. Takhistov, *Phys. Rev. Lett.* **119**, 061101 (2017).
- [94] C. Keith, D. Hooper, N. Blinov, and S. McDermott, *Phys. Rev. D* **102**, 103512 (2020).
- [95] M. Kawasaki, A. Kusenko, and T. Yanagida, *Phys. Lett. B* **711**, 1 (2012).
- [96] X. Wang, Y. Zhang, R. Kimura, M. Yamaguchi, *Sci. China Phys. Mech. Astron.* **66**, 260462 (2023).
- [97] K. Inomata, M. Kawasaki, K. Mukaida, Y. Tada, and T. Yanagida, *Phys. Rev. D* **95**, 123510 (2017).

- [98] D. Page, Phys. Rev. D **13**, 198 (1976).
- [99] F. Kuhnel and K. Freese, Phys. Rev. D **95**, 083508 (2017).
- [100] B. Carr, M. Raidal, T. Tenkanen, V. Vaskonen, and H. Veermae, Phys. Rev. D **96**, 023514 (2017).
- [101] R. D'Agostino, R. Giambo, and O. Luongo, Phys. Rev. D **107**, 043032 (2023).
- [102] A. Green, Nuclear Physics B **1003**, 116494 (2024).
- [103] S. Hsu, Phys. Lett. B **594** 13 (2004).
- [104] R. Horvat, Phys. Rev. D **70** 087301 (2004).
- [105] M. Li, Phys. Lett. B **603** 1 (2004).
- [106] E. Witten, Adv. Theor. Math. Phys. **2** 253 (1998).
- [107] R. Bousso, Rev. Modern Phys. **74** 825 (2002).
- [108] J. D. Barrow, Phys. Lett. B **808** 135643 (2020).
- [109] E. N. Saridakis, Phys. Rev. D **102** 123525 (2020).
- [110] F. K. Anagnostopoulos, S. Basilakos, and E. N. Saridakis, Eur. Phys. J. C **80** 826 (2020).
- [111] S. Srivastava and U. K. Sharma, Int. J. Geom. Methods Mod. Phys. **18** 2150014 (2021).
- [112] A. Sheykhi, Phys. Rev. D **103**, 123503 (2021).
- [113] A. Oliveros, M. Sabogal, and M. Acero, Eur. Phys. J. Plus **137**, 783 (2022).
- [114] Q. Huang, H. Huang, B. Xu, F. Tu, and J. Chen, Eur. Phys. J. C **81**, 686 (2021).
- [115] P. Adhikary, S. Das, S. Basilakos, and E. Saridakis, Phys. Rev. D **104**, 123519 (2021).
- [116] A. Mamon, A. Paliathanasis, and S. Saha, Eur. Phys. J. Plus **136**, 134 (2021).
- [117] S. Rani and N. Azhar, Universe **7**, 268 (2021).
- [118] G. Luciano, Phys. Rev. D **106**, 083530 (2022).
- [119] S. Nojiri, S. Odintsov, and T. Paul, Phys. Lett. B **825**, 136844 (2022).
- [120] B. Paul, B. Roy, and A. Saha, Eur. Phys. J. C **82**, 76 (2022).
- [121] N. Boulkaboul, Phys. Dark Univ. **40**, 101205 (2023).
- [122] R. Pankaj, U. Sharma, and N. Ali, Astrophys Space Sci. **368**, 15 (2023).
- [123] S. Ghaffari, G. Luciano, and S. Capozziello, Eur. Phys. J. Plus **138**, 82 (2023).
- [124] G. Luciano, Eur. Phys. J. C **83**, 329 (2023).

- [125] M. Asghari and A. Sheykhi, *Eur. Phys. J. C* **82**, 388 (2022).
- [126] K. Jusufi, M. Azreg-Ainou, M. Jamil, and E. Saridakis, *Universe* **8**, 102 (2022).
- [127] J. Barrow, S. Basilakos, and E. Saridakis, *Phys. Lett. B* **815**, 136134 (2021).
- [128] F. Anagnostopoulos, S. Basilakos, and E. Saridakis, *Eur. Phys. J. C* **80**, 826 (2020).
- [129] J. Barrow, *Phys. Lett. B* **808**, 135643 (2020).
- [130] S. Nojiri, S. Odintsov, and V. Oikonomou, *Phys. Rep.* **692**, 1 (2017).
- [131] J. Hwang and H. Noh, *Phys. Rev. D* **71**, 063536 (2005).
- [132] A. Linde, *Phys. Lett. B* **129**, 177 (1983).
- [133] Planck Collaboration, *A&A* **641**, A6 (2020).
- [134] K. Freese, J. Frieman, and A. Olinto, *Phys. Rev. Lett.* **65**, 3233 (1990).
- [135] F. Adams, J. Bond, K. Freese, J. Frieman, and A. Olinto, *Phys. Rev. D* **47**, 426 (1993).
- [136] L. Boubekeur and D. Lyth, *JCAP* **07**, 02 (2005).
- [137] H. Motohashi and W. Hu, *Phys. Rev. D* **96**, 063503 (2017).
- [138] S. Young, C. Byrnes, and M. Sasaki, *JCAP* **07**, 045 (2014).
- [139] Y. Tada and S. Yokoyama, *Phys. Rev. D* **100**, 023537 (2019).
- [140] I. Musco and J. Miller, *Class. Quantum Gravi.* **30**, 145009 (2013).
- [141] T. Harada, C. Yoo, and K. Kohri, *Phys. Rev. D* **88**, 084051 (2013); **89**, 029903(E) (2014).
- [142] R. Cai, Z. Guo, J. Liu, L. Liu, and X. Yang, *JCAP* **06**, 013 (2020).
- [143] D. Fixsen, E. Cheng, J. Gales, J. Mather, R. Shafer, and E. Wright, *Astrophys. J.* **473**, 576 (1996).
- [144] K. Inomata, M. Kawasaki, and Y. Tada, *Phys. Rev. D* **94**, 043527 (2016).
- [145] K. Inomata and T. Nakama, *Phys. Rev. D* **99**, 043511 (2019).
- [146] B. Carr, K. Kohri, Y. Sendouda, and J. Yokoyama, *Phys. Rev. D* **81**, 104019 (2010).
- [147] P. Graham, S. Rajendran, and J. Varela, *Phys. Rev. D* **92**, 063007 (2015).
- [148] R. Laha, *Phys. Rev. Lett.* **123**, 251101 (2019).
- [149] K. Griest, A. Cieplak, and M. Lehner, *Phys. Rev. Lett.* **111**, 181302 (2013).
- [150] H. Niikura, M. Takada, S. Yokoyama, T. Sumi, and S. Masaki, *Phys. Rev. D* **99**, 083503 (2019).

- [151] P. Tisserand, L. Le Guillou, C. Afonso, et al. (EROS-2 Collaboration), *Astron. Astrophys.* **469**, 387 (2007).
- [152] V. Poulin, P. Serpico, F. Calore, S. Clesse and K. Kohri, *Phys. Rev. D* **96**, 083524 (2017).
- [153] S. Hawking, *Nature* **248**, 30 (1974).
- [154] A. Coogan, L. Morrison, and S. Profumo, *Phys. Rev. Lett.* **126**, 171101 (2021).
- [155] D. Page, *Phys. Rev. D* **13**, 198 (1976).
- [156] B. Nayak and L. Singh, *Pramana* **76**, 173 (2011).
- [157] M. Jamil and A. Qadir, *Gen. Relativ. Gravit.* **43**, 1069 (2011).
- [158] E. Babichev, V. Dokuchaev, and Y. Eroshenko, *Phys. Rev. Lett.* **93**, 021102 (2004).
- [159] B. Nayak and L. Singh, *Phys. Rev. D* **82**, 127301 (2010).